

# Structural Evolution of Pt, Au and Cu Anodes by Electrolysis up to Contact Glow Discharge Electrolysis in Alkaline Electrolytes\*\*

Evelyn Artmann,<sup>[a]</sup> Pramod V. Menezes,<sup>[a]</sup> Lukas Forschner,<sup>[a]</sup> Mohamed M. Elnagar,<sup>[a]</sup> Ludwig A. Kibler,<sup>[a]</sup> Timo Jacob,<sup>\*[a]</sup> and Albert K. Engstfeld<sup>\*[a]</sup>

Applying a voltage to metal electrodes in contact with aqueous electrolytes results in the electrolysis of water at voltages above the decomposition voltage and plasma formation in the electrolyte at much higher voltages referred to as contact glow discharge electrolysis (CGDE). While several studies explore parameters that lead to changes in the  $I-U$  characteristics in this voltage range, little is known about the evolution of the structural properties of the electrodes. Here we study this aspect on materials essential to electrocatalysis, namely Pt, Au, and Cu. The stationary  $I-U$  characteristics are almost identical for all electrodes. Detailed structural characterization by optical

microscopy, scanning electron microscopy, and electrochemical approaches reveal that Pt is stable during electrolysis and CGDE, while Au and Cu exhibit a voltage-dependent oxide formation. More importantly, oxides are reduced when the Au and Cu electrodes are kept in the electrolysis solution after electrolysis. We suspect that  $H_2O_2$  (formed during electrolysis) is responsible for the oxide reduction. The reduced oxides (which are also accessible *via* electrochemical reduction) form a porous film, representing a possible new class of materials in energy storage and conversion studies.

## 1. Introduction

Applying a voltage to metal electrodes in contact with aqueous electrolytes is used to catalyze Faraday and non-Faraday reactions,<sup>[1–3]</sup> tailor surface properties of electrodes,<sup>[4–7]</sup> form nanoparticles<sup>[8,9]</sup> or alter the electrolyte composition,<sup>[1,7]</sup> as well as to ignite plasmas in solution.<sup>[1,10,11]</sup> Depending on the application, a detailed understanding of the parameters that limit the electrode stability is decisive to prevent material degradation or to adjust the formation of specific structures. The electrode stability is highly dependent on the applied voltage and the processes occurring at the electrode surface, which change dramatically when the voltage is increased significantly. Focusing on gas-evolving working electrodes, the phenomena that are expected to occur at the solid|liquid interface can be summarized as follows. For voltages above the decomposition voltage of water (low voltages), water electrolysis is observed (referred to as normal electrolysis – NE).


Increasing the voltage leads to violent bubble formation until the so-called breakdown voltage ( $V_b$ ), where a gas film (sheath) forms around the electrode. At even higher voltages, the formation of a homogeneous plasma is observed within this sheath, which is called contact glow discharge electrolysis (CGDE).<sup>[1,10–12]</sup> The voltage at which CGDE is formed (minimum of the  $I-U$  curve) is called the midpoint voltage ( $V_D$ ).


Since the discovery of CGDE in aqueous electrolytes by H. Kellogg in 1950,<sup>[10]</sup> there have been several reports describing the shape of current-voltage ( $I-U$ ) curves from NE to CGDE, exploring the impact of electrode material, electrolyte, temperature, pH, composition, electrode geometry, etc.<sup>[1,9,11–16]</sup> The most noteworthy observation for the present work is that during CGDE, the products formed at the interface are more diverse than those known from NE. For example, regardless of electrode polarity, both  $H_2$  and  $O_2$  may be formed simultaneously during CGDE. More importantly, in anodic CGDE, in addition significant amounts of  $H_2O_2$  are also produced.<sup>[11,12,17]</sup> The origin of the formation of the product cocktail is caused by non-Faraday processes, where  $H_2O$  molecules decompose into highly reactive short-lived radicals and ions during CGDE, which react one with another in the plasma phase or at the plasma|liquid interface.<sup>[1,12,18]</sup>

Less is known on the evolution of the structural properties of the electrode material with increasing voltage from the NE to the CGDE regime.<sup>[6]</sup> Instead, the structural properties for both limiting regions are usually studied separately, for different reasons which is illustrated by the following examples. For the NE region electrode stability is an important aspect in electrocatalysis. Stable electrodes during the reaction are desired since degradation of the catalyst often lowers the efficiency. Besides, anodizing electrodes in aqueous electrolytes is used to form

[a] E. Artmann, Dr. P. V. Menezes, L. Forschner, M. M. Elnagar, Dr. L. A. Kibler, Prof. Dr. T. Jacob, Dr. A. K. Engstfeld  
Institute of Electrochemistry, Ulm University, D-89081 Ulm, Germany  
Phone: +49 (0)731 25401, Fax: +49 (0)731 25409  
E-mail: timo.jacob@uni-ulm.de  
albert.engstfeld@uni-ulm.de

[\*\*] A previous version of this manuscript has been deposited on a preprint server (<https://doi.org/10.26434/chemrxiv.14721111.v1>)

 Supporting information for this article is available on the WWW under <https://doi.org/10.1002/cphc.202100433>

 © 2021 The Authors. ChemPhysChem published by Wiley-VCH GmbH. This is an open access article under the terms of the Creative Commons Attribution Non-Commercial License, which permits use, distribution and reproduction in any medium, provided the original work is properly cited and is not used for commercial purposes.

oxide structures or to smooth or clean materials *via* electropolishing.<sup>[4,19]</sup> Strong negative polarization in turn can lead to corrosion of the cathode.<sup>[8,20–22]</sup> This approach can produce nanoparticles, tune the surface crystallographic orientation for catalytic reactions or other applications.<sup>[8,20–22]</sup> Investigating the high-voltage regime, where plasmas can be generated in liquid is a growing area of research, aiming at a fundamental understanding of plasma formation, its interaction with the solid electrode and the electrolyte, as well as exploring new fields of application.<sup>[5–7,18,23]</sup> Plasmas in liquid can be used to distinctly tailor the (near-)surface electrode properties, *i. e.*, to form durable oxide coatings on materials of complex sizes *via* plasma electrolytic oxidation (PEO)<sup>[24–26]</sup> or to remove irregularities from the workpiece *via* plasma electrolytic polishing (PEP).<sup>[6,27]</sup> As with cathodic corrosion, the electrodes can also decompose into (multi-)metallic or oxidic nanoparticles.<sup>[7,9,23,28–33]</sup> Such particles can also be formed from metal ions present in the electrolyte during plasma electrolysis.<sup>[7,34]</sup> Finally, another interesting and yet emerging field is the wastewater treatment by plasmas,<sup>[7,23,35–37]</sup> where the stability of the prepared electrodes is detrimental to prevent any kind of metal contamination in the water. These examples and applications show the broad application of plasma treatment and the importance of having a clear picture of any kind of plasma-induced structure changes or formation processes. Overall, the examples also raise the question if similar or other structures to those observed in the NE and CGDE regime, are accessible in the voltage regime in between.

This is subject of this work, which aims at providing (i) more detailed and systematic insights into possible changes in the structural properties of gas-evolving metal electrodes and (ii) new approaches for material design, covering the voltage range from NE to CGDE. Motivated by their importance in electrochemistry and electrocatalysis, we restrict our investigations to processes at poly-crystalline Pt,<sup>[38–42]</sup> Au<sup>[43–45]</sup> and Cu<sup>[46–48]</sup> wire anodes. While various studies have addressed the structure of these electrodes at low potentials (NE regime), much less is known about their behavior during CGDE.<sup>[7,9–11,31,32,49]</sup> Au is the most noble metal and is used extensively as a model electrode in electrochemical surface science.<sup>[43,44]</sup> Despite its nobility, Au was shown to form Au<sub>2</sub>O<sub>3</sub> films on its surface for low potentials before and in the oxygen evolution reaction (OER) region.<sup>[45]</sup> These Au<sub>2</sub>O<sub>3</sub> films are, however, chemically unstable at room temperature.<sup>[50]</sup> Reports on the structural properties of Au beyond NE are rare,<sup>[11]</sup> and primarily focus on cathodic CGDE, where Au nanoparticles are formed.<sup>[31,32,49]</sup> Cu raised a lot of interest in the electrocatalysis community during recent decades as it is the only pure metal that converts CO<sub>2</sub> electrochemically into higher valuable hydrocarbons. This is an important process in the decarbonization of society and closing the carbon cycle.<sup>[7,48]</sup> There exists a plethora of different approaches to prepare Cu catalyst materials.<sup>[51]</sup> Among those, it was reported that nanostructured Cu electrode materials can be prepared *via* gas phase plasma oxidation.<sup>[47]</sup> A direct preparation of catalytically active surfaces *via* CGDE could provide an alternative approach for *in situ* preparation of the catalyst material. Similar to Au, Cu electrodes used under CGDE

conditions were primarily studied for the purpose of nanoparticle formation.<sup>[7,9]</sup> In our study, the electrodes are investigated by potentiostatic electrolysis at a set of voltages ranging from the NE region up to 580 V in 0.01 M KOH electrolyte. The resulting *I–U* behavior is discussed based on the structural properties investigated after the electrolysis. The topography and microscopic changes of the electrodes are imaged with an optical microscope and by scanning electron microscopy (SEM). For the oxide-forming metals Au and Cu, the amount of oxide formed during electrolysis is subsequently determined from chronoamperometric measurements performed at potentials below the reduction potential of the respective oxides. We demonstrate, that independent of the applied voltage during electrolysis (50 to 580 V), the Au and Cu oxides are also reduced when kept in the electrolysis solution after the electrolysis. The effect of H<sub>2</sub>O<sub>2</sub> on the oxide reduction is discussed. Finally, we demonstrate that the oxide reduction leads to the formation of highly porous nanostructures, determined from combined cyclic voltammetry and SEM experiments.

## 2. Results and Discussion

In the following, first the *I–U* behavior of the different investigated metals is discussed, followed by detailed analysis of their rather specific and divergent structural and electrochemical properties. The general observations for all systems are finally summarized in the conclusion. A detailed description of the experimental conditions is provided at the end of the manuscript and further details are provided in the supporting information (SI).

### 2.1. *I–U* Characteristics

Figure 1 shows stationary *I–U* characteristics of Pt, Au, and Cu wire electrodes (immersed length 10 mm, diameter 0.5 mm) recorded for 30 s electrolysis in 0.01 M KOH where the averaged current density values for each voltage were obtained with freshly prepared electrodes. The chronoamperometric curves for the individual values are provided in Figure S1. Longer electrolysis times were avoided to prevent significant changes in electrolyte temperature, which can change the *I–U* behavior significantly. For a similar reason, applying voltages above 580 V was avoided, where in addition the wire can easily melt. Details on the experimental approach, chronoamperometric measurements, data evaluation, and the effect of temperature are provided in the experimental section and the supporting information (Figures S1 and S2).

The *I–U* behavior in Figure 1 is characteristic for gas-evolving electrodes.<sup>[11,15,52]</sup> In the NE region from approximately 50 V up to  $V_B$  at ca. 350 V, the current increases linearly due to the limited conductivity of the electrolyte according to Ohm's law.<sup>[11,12,52]</sup> Note that at low overpotentials (few volts), electrolysis is limited by the activation of charge transfer that usually leads to an exponential increase of the current density.

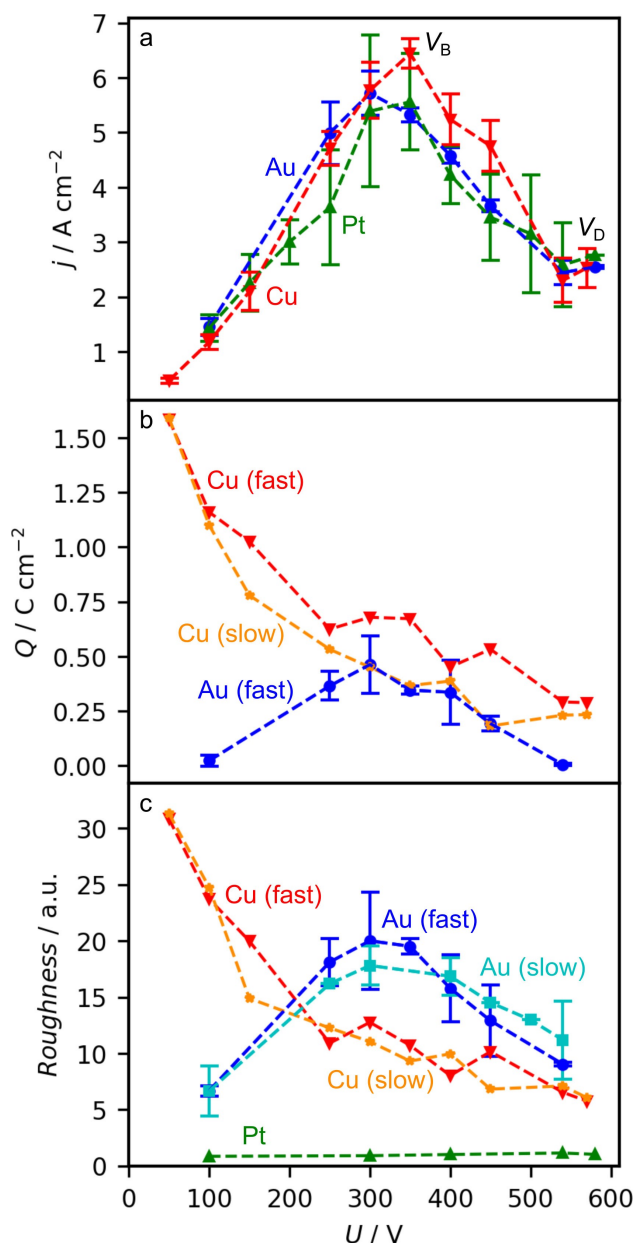


**Figure 1.** a)  $I$ - $U$  characteristics, where each data point was recorded with a freshly prepared electrode for 30 s electrolysis in 0.01 M KOH. b) Cathodic charge density determined from the chronoamperometry measurements in Figure 6 and Figure 10 for Au and for Cu, respectively, recorded after the electrolysis and subsequent electrochemical reduction. It is important to distinguish whether the electrode is removed immediately after the electrolysis from the solution (fast) or kept in the electrolysis solution for additional 60 s (slow). c) Change in roughness factor (RF) with respect to the as-prepared samples after the anodic polarization and subsequent electrochemical reduction determined from the CVs presented in Figure 7 for Au, and Figure 11 for Cu.

At  $V_B$  the resistance increases due to gas film formation around the electrode, which leads to a breakdown of the NE concomitant with a decrease in current density. The effect becomes more pronounced with increasing voltage. Close to  $V_D$  at ca. 540 V, sparks are observed by visual inspection in the gas film forming around the electrode. At  $V_D$  the electrode is

completely wrapped in a gas sheath and a blue-violet fast fluctuating plasma with an electrifying, sharply hissing sound is observed within the sheath.

Overall, the  $I$ - $U$  characteristics are very similar for all three electrode materials investigated, and the current densities at the characteristic voltages  $V_B$  and  $V_D$  are almost identical. This suggests that for a given electrolyte the  $I$ - $U$  behavior is almost independent of the examined electrode material and that the material properties (i) do not change, (ii) change in a similar fashion, or (iii) changes of the material properties are not important for the  $I$ - $U$  curves.

A direct comparison of the current values at specific voltages, specifically the occurrence of characteristic voltages ( $V_B$  and  $V_D$ ), with results from literature is, however, not straightforward. As mentioned above, in general the  $I$ - $U$  behavior strongly depends on the experimental conditions, and furthermore the values of the characteristic voltages strongly depend on the cell and electrode geometry.<sup>[1,9,11–16,53]</sup> Nevertheless, Hickling and Ingram investigated the  $I$ - $U$  behavior of Pt, Au and Cu wire electrodes (among others), although in another electrolyte (0.05 M  $Na_2HPO_4$ ). These results showed that Au, Pd, and Pt show a very similar behavior during electrolysis at various voltages compared to W, Cu, or NiCr.<sup>[11]</sup> The authors suggested that on the latter metals oxide film formation and corrosion are at the origin of the different behavior compared to Au, Pd and Pt.<sup>[11]</sup> Our results on the structural properties of the electrodes discussed below, will show that oxide formation occurs on Au and Cu electrodes. The fact that the  $I$ - $U$  curves of Au and Cu are almost identical to that of Pt, suggests that the electron transport through the oxide film on Au and Cu is equally fast as for bare Pt electrodes, which is different for systems that form passive oxide films.<sup>[15]</sup>

## 2.2. Structure Formation

Further insights on the impact of the electrolysis on the structural properties of the electrodes are gained from optical microscopy, SEM, and detailed voltammetric studies of the electrodes, by comparing the data recorded before and after electrolysis. While the microscope images (optical and SEM) provide insights into the three-dimensional structural changes, from the cyclic voltammetry measurements we can additionally deduce (i) the amount of oxide formed during electrolysis, (ii) determine possible changes in the crystallographic orientation of the surface, and (iii) derive changes in surface area.<sup>[54,55]</sup> In the following, the electrode materials are discussed separately since the structural modifications of the investigated metals differ strongly one from another.

### 2.2.1. Platinum

The SEM images of an as-prepared Pt wire and that after the electrolysis at 300 V for 30 s in 0.01 M KOH are depicted in Figure 2. Further images obtained for other electrolysis voltages (100 and 580 V) are provided in Figure S3. The SEM images

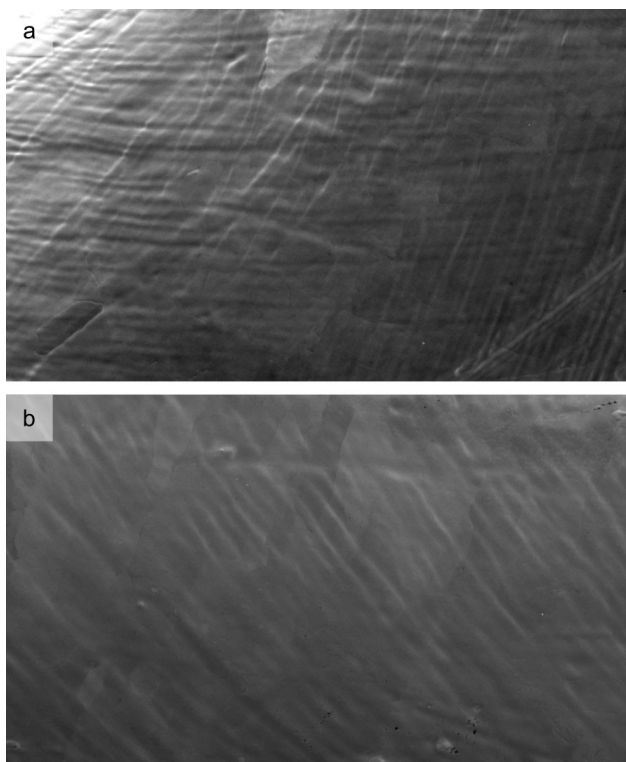


**Figure 2.** SEM images ( $250\ \mu\text{m} \times 150\ \mu\text{m}$ ) of a Pt wire electrode a) as-prepared and b) after electrolysis at 300 V for 30 s in 0.01 M KOH. Further SEM images are provided in Figure S3. The images were improved by adjusting the contrast and brightness.

suggest that the Pt surface does not restructure significantly during electrolysis at any applied voltage.

To substantiate this finding, we studied the electrodes by cyclic voltammetry. The cyclic voltammograms (CVs) recorded for the Pt electrodes in 0.01 M KOH at  $50\ \text{mVs}^{-1}$  before (black) and after electrolysis (blue & orange) are presented in Figure 3. All potentials in the electrochemical experiments are on the

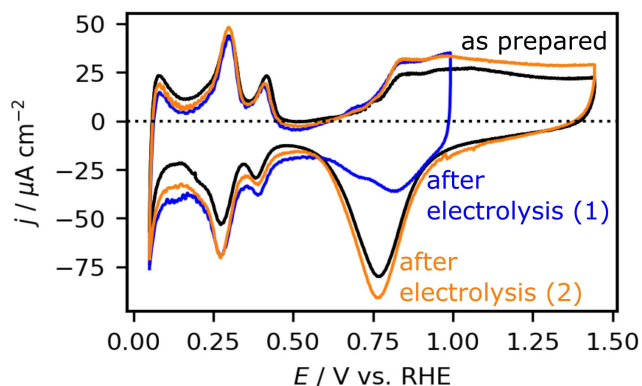


**Figure 3.** CVs of an as-prepared Pt electrode recorded in 0.01 M KOH at  $50\ \text{mVs}^{-1}$  (black curve) and the same electrode after the electrolysis at 300 V for 30 s in 0.01 M KOH. The first CV after the electrolysis was recorded with an upper potential limit of 1.0 V (blue). Subsequently, additional cycles were recorded with an upper potential limit of 1.45 V (orange).

reversible hydrogen electrode (RHE) scale unless otherwise mentioned. The CVs show the typical features for hydrogen ad-/desorption (between 0.05 and 0.55 V) and OH/O ad-/desorption (between 0.7 and 1.0 or 1.5 V) on Pt in alkaline electrolytes.<sup>[56]</sup> The downshift of the current density in the hydrogen region is caused by residual oxygen in the cell. For the first voltammetric cycle recorded after the electrolysis (blue), the upper potential limit was fixed at 1.0 V to avoid significant surface restructuring which would occur by applying higher potentials.<sup>[57–60]</sup> The CV recorded with an upper potential limit of 1.45 V (orange) was subsequently recorded.

The voltammetric peaks are located at almost the same potentials, and also the current densities at the peak maxima are rather similar, hence the crystallographic orientation of the surface did not change measurably. The small changes in the current density are within the limits of the experimental precision. This may be because the immersion depth of the wires cannot always be set precisely the same. Nevertheless, the almost identical current-potential profiles in the CVs recorded before and after the electrolysis suggest that the surface area does not change significantly. Henceforth, the change in electrochemical surface area is denoted as roughness factor (RF), which is described in detail in the experimental section. For Pt the RF remains almost at unity, as shown in Figure 1c (green triangles). Note that much more sensitive methods are needed to resolve possible restructuring processes on the atomic scale. For the high voltage region (CGDE), Pt was previously suggested to be stable in a wide range of electrolytes.<sup>[10,11,13,61–63]</sup> Interestingly, gas phase plasma treatment with oxygen also does not roughen the electrode surface, but leads to the formation of a Pt-oxide.<sup>[64]</sup> This is different in the OER region (onset of NE in the range of a few volts which was not investigated in this study), where surface restructuring has been suggested by Favaro *et al.*<sup>[65]</sup> Studying the OER on Pt electrodes in alkaline electrolytes, the authors observed a restructuring of the electrodes with *ex situ* atomic force microscopy (AFM) after the OER. They also observed the formation of a complex, several nm thick oxy-hydroxy film on the electrode surface, as elucidated by using ambient pressure X-ray photoelectron spectroscopy (APXPS).<sup>[65]</sup> Bulk oxide formation under these conditions was also suggested by theoretical studies to be thermodynamically favorable at high overpotentials for Pt nanoparticles.<sup>[66]</sup> From experiments the oxidation of Pt electrodes was, however, suggested to be kinetically limited and hence the formation of thick oxide films is slowed down due to the short electrolysis times.<sup>[67]</sup>

From studying the first negative potential scan of the CV starting from 0.95 V in our experiment, we did not observe any currents related to oxide reduction. Even though we cannot completely rule out that the surfaces reduce during the transfer from one cell to another, we suggest that in our experiment oxide formation does not occur during electrolysis at voltages above 100 V in alkaline electrolyte.

### 2.2.2. Gold

After performing electrolysis at different voltages for 30 s in 0.01 M KOH (as in Figure 1a), inspection of the Au electrodes by the naked eye revealed a color change for all voltages. In addition, the intensity and color depends on the applied voltage and more importantly on the time of exposure of the electrode to the electrolyte after the electrolysis. This is demonstrated by the optical microscope image in Figure 4 for a Au electrode on which 300 V were applied during electrolysis. If the electrode is immediately removed from the electrolyte after electrolysis the electrode is red (region 1), whereas the electrode part that was kept in the electrolysis solution turns black within a few seconds (region 3). Respective microscope images taken after the electrolysis at different voltages are provided in Figures 5a to d (first column) along with selected SEM images recorded on the red region (1), transition region (2), and black region (3) in the second to the fourth column. Overall, the red color of the Au wire suggests that a  $\text{Au}_2\text{O}_3$  layer is formed during the electrolysis on the electrode. Considering that  $\text{Au}_2\text{O}_3$  was also observed for oxygen plasma treated Au electrodes,<sup>[68,69]</sup> it is very likely that  $\text{Au}_2\text{O}_3$  is formed especially in the CGDE region, where oxygen species are present in the plasma. For comparison with the initial surface structure of the Au electrode, a SEM image of the as-prepared Au electrode is provided in the SI (Figure S4a).

Focusing on the red part (region 1), obtained by electrolysis and subsequently direct removal of the electrode from the electrolyte solution, we observe in the optical microscope images that the intensity of the red color varies with the applied voltage. At 300 and 400 V the red tone is rather intense, while at 100 and 540 V the red color is less pronounced and shows a touch of orange. Corresponding SEM images are provided in Figures 5e to h (second column). For all voltages, the surface shows large flat regions and several approximately 150 nm wide cracks. In some regions, it seems as if the newly formed adlayer peels off from the Au wire substrate. While the origin of this process is unclear, we suggest that this can be caused by the emersion and immersion of the electrode during the transfer between the different electrochemical cells. The holes observed in the SEM images, especially in Figures 5e–g, are primarily induced by the electron beam of the SEM (see Figure S5).

The amount of oxide formed during electrolysis was quantified by electrochemical reduction in 0.01 M KOH, as shown in Figure 6. Here the potential was swept at  $50 \text{ mVs}^{-1}$  from an initial potential of 1.10 V to 0.25 V, where the potential was kept until the reduction current became insignificant (up to 50 s). The total charge passed during these chronoamperometry measurements is depicted in Figure 1b. The trend in charge density passed in each measurement follows the  $I-U$  behavior in Figure 1a, where the largest charge density is obtained for electrolysis at 300 V with  $460 \text{ mCcm}^{-2}$ . For voltages around 100 V and 540 V the amount of oxide is significantly lower, with ca.  $23 \text{ mCcm}^{-2}$  at 100 V and  $6 \text{ mCcm}^{-2}$  at 540 V.

Considering that the charge density is related to the amount of oxide formed per  $\text{cm}^2$  during 30 s of electrolysis, the thickest oxide film is formed at around 300 V. Another important observation is that the initially red electrode turned black during the reduction process. SEM imaging of these reduced electrodes revealed a highly porous structure which is depicted in Figure S6. Such a change in color has been reported recently for the reduction of  $\text{Au}_2\text{O}_3$  to metallic Au,<sup>[70]</sup> and the black color has been attributed to the ability of the nanostructured Au surface to absorb significantly the incident light from the visible spectrum.<sup>[71,72]</sup>

Comparing the CV of an as-prepared Au wire electrode (Figure 7a) with those obtained after the electrolysis and subsequent electrochemical reduction in Figure 7b, overall higher current densities are observed for the latter electrodes. Note that all current densities are normalized to the initial geometric surface area of the wire. No additional peaks or changes in relative peak sizes are observed in the CVs, which would indicate a change of surface structure or crystallographic orientation.<sup>[21,22]</sup> The shift of the oxidation (reduction) peaks to more positive (negative) potentials for higher current densities is presumably caused by internal resistance effects. The increase in Faraday current suggests a strong increase in surface area, especially for electrolysis at around 300 V, which is apparent from the change in RF shown in Figure 1c (labeled Au fast). The evolution of the RF after reduction of the  $\text{Au}_2\text{O}_3$  phase formed during the electrolysis with increasing voltage follows the overall trend of the  $I-U$  and  $Q-U$  curves of Figures 1a and b, where the highest RF value is obtained at  $V_B$  (ca. 300 V). Interestingly, for electrolysis at 100 and 540 V, where the amount of surface oxide was low (Figure 1b), the increase in surface area is still significant but lower than at  $V_B$ . Possible

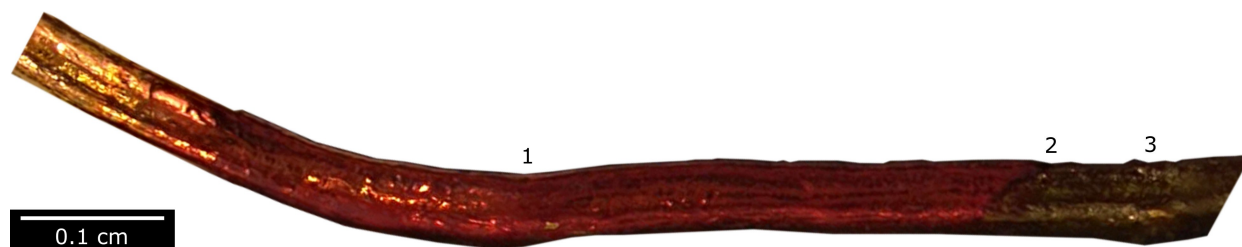


**Figure 4.** Microscope image of a Au wire after electrolysis at 300 V for 30 s in 0.01 M KOH. The left (golden) part shows the as-prepared Au wire, the middle (red) part (region 1) was immediately removed from the electrolyte after the electrolysis, and the right (black) part (region 3) was kept in the electrolysis solution for 60 s after switching the voltage off. Region 2 marks the transition between regions 1 and 3.

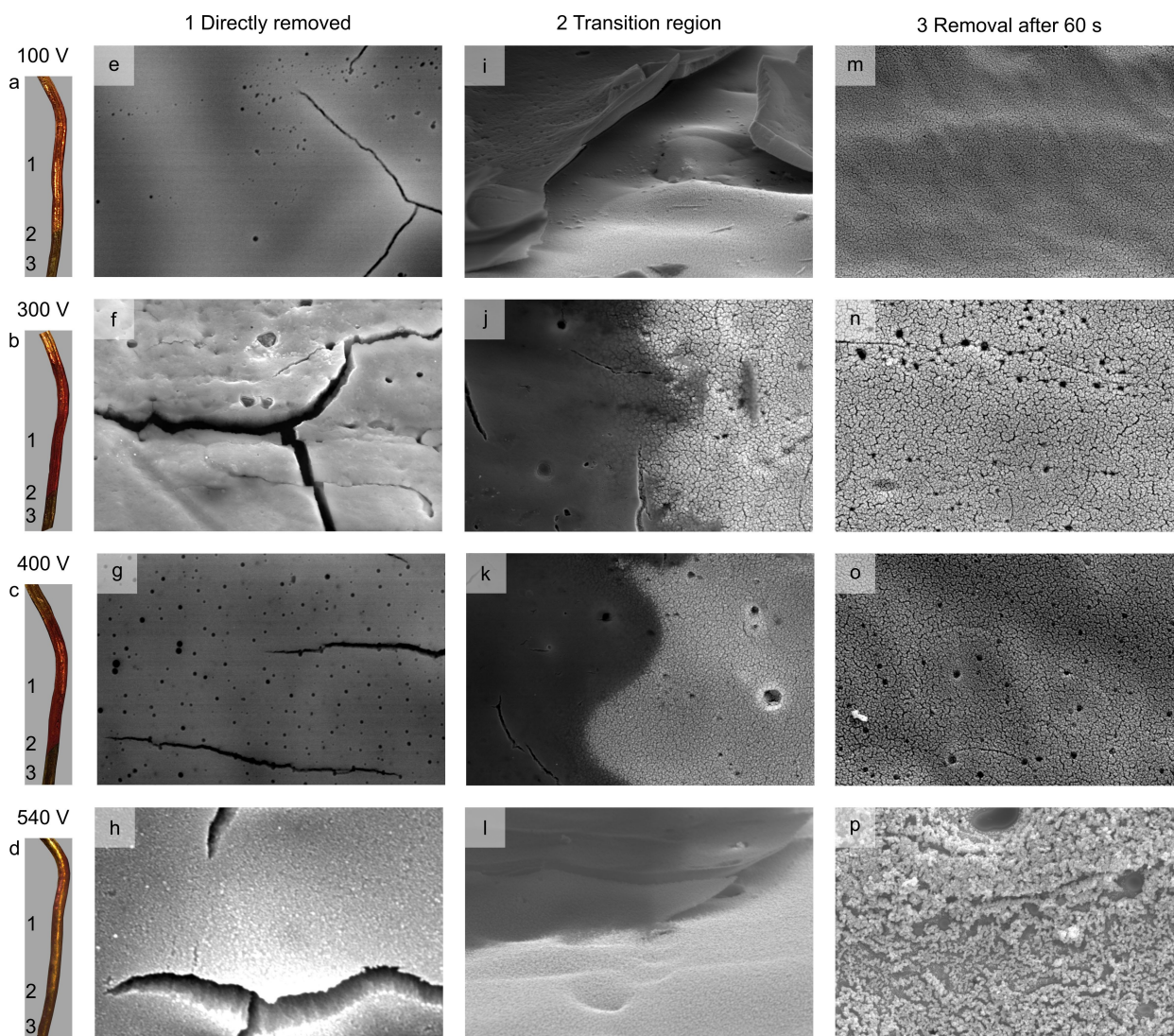


**Figure 5.** Left column: Optical microscope images of Au wires taken after electrolysis at the given voltages for 30 s in 0.01 M KOH. The numbers in the optical microscope images (a–d) illustrate the different regions in Figure 4. The second to fourth column show from left to right SEM images of the regions 1–3 ( $12\ \mu\text{m} \times 8\ \mu\text{m}$ ), recorded after electrolysis at different voltages. A SEM image of an as-prepared electrode is provided in Figure S4a.

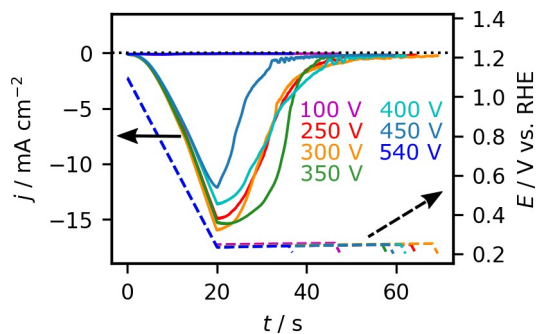


**Figure 6.** Characterization of the amount of oxide formed on Au wires after electrolysis in 0.01 M KOH at the given voltages. The potential was swept at  $50\ \text{mVs}^{-1}$  from the initial potential of 1.1 V to 0.25 V, where the potential was held until the cathodic current became insignificant.

reasons for the voltage-dependent growth rates are yet to be resolved.

A peculiar observation is that the Au electrodes also turn black when they are kept in the electrolysis solution for 60 s after the electrolysis (see region 3 in Figure 4). Unlike for the red part (region 1), the intensity of the color is similar for all voltages. Corresponding SEM images are provided in Figures 5m–p (fourth column). Compared to the red part of the electrode, the surface is much more porous, with a sponge-like surface structure that looks very similar to that obtained after the electrochemical reduction of the  $\text{Au}_2\text{O}_3$ . For a better comparison between the structures, in Figures 5i–l (third column) we depict the transition region (region 2) between the red and black parts. In these images, the red  $\text{Au}_2\text{O}_3$  region appears darker than the black nanoporous metallic Au region.

Inspection of the black region by cyclic voltammetry did not show any signs of surface or near-surface oxide reduction in the

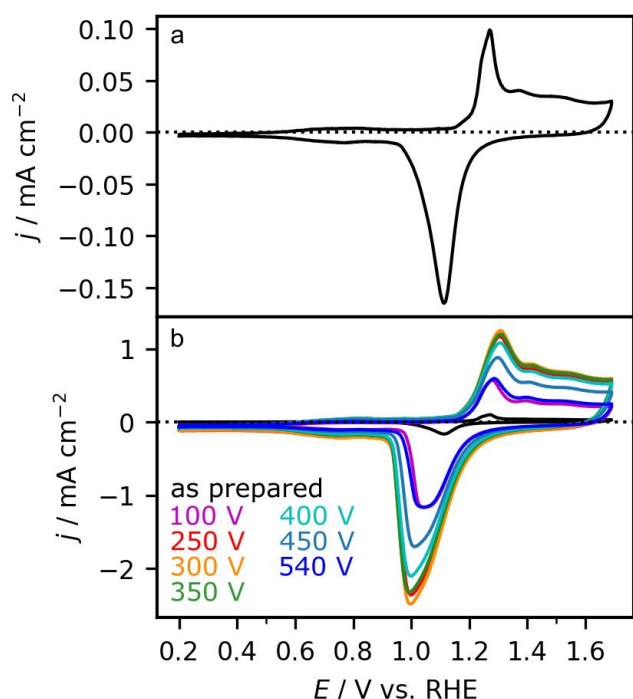


**Figure 7.** CVs of a) an as-prepared Au wire in 0.01 M KOH (black) and b) the same electrode in comparison to the electrochemically reduced electrodes in Figure 6 (previously treated by electrolysis at the given voltages). The CVs were recorded at  $50 \text{ mV s}^{-1}$ .

first negative-going scan in contrast to the red part of the Au wire. Instead, the CVs look almost identical to those obtained after electrochemical reduction of the red electrodes shown in Figure 7b, and also the RF is almost identical to those obtained for the red electrodes polarized at similar voltages (Figure 1c – labelled Au slow).

To elucidate the origin of the color change of the Au electrodes kept in the electrolysis solution, we first stored electrodes directly removed from the electrolysis solution under ambient conditions or in a fresh 0.01 M KOH solution for 24 to 48 hours. This did not induce a color change, and hence, the structural change had to be caused by species present in the solution after electrolysis. For low voltages (NE), it is expected that mainly  $\text{O}_2$  is formed from water splitting. At significantly high voltages, in the region of CGDE (in our case  $> 540 \text{ V}$ ), it has been demonstrated that after the electrolysis in addition to  $\text{O}_2$ , also  $\text{H}_2$  and  $\text{H}_2\text{O}_2$  are present in the electrolyte.<sup>[11,17,61]</sup> In a further

set of experiments, the Au electrodes that were removed immediately after electrolysis, were dipped into KOH solutions saturated with  $\text{H}_2$ ,  $\text{O}_2$ , or mixed with  $\text{H}_2\text{O}_2$ . We could only observe a color change from red to black in the  $\text{H}_2\text{O}_2$  containing solution. Hence it is reasonable to assume that the  $\text{H}_2\text{O}_2$  is at the origin of the reduction process at least at high voltages. To what extent highly-reactive, short-living or excited radicals and ions, present during and shortly after CGDE, contribute to the reduction process after the electrolysis can not be deduced from our experiments. The origin of the oxide reduction at lower voltages in the electrolysis solution can only be speculated on, and further experiments are required to elucidate whether  $\text{H}_2\text{O}_2$  possibly forms under these experimental conditions.

### 2.2.3. Copper

As in the case of Au, for Cu electrodes also the impact of removing the electrodes immediately after the electrolysis from the electrolyte and after keeping the electrodes for additional 60 s in the electrolysis solution was investigated. Independent of the experimental procedure, the Cu electrodes turned black. Only with the optical microscope subtle color changes are observed on a wire treated by both approaches, as shown in Figure 8. The color changes were independent of the applied voltage during electrolysis. The black color strongly implies that a Cu(II)-oxide ( $\text{CuO}$ ) is formed. Note that Cu(I)-oxide ( $\text{Cu}_2\text{O}$ ) is red. The formation of Cu oxides with different oxidation states was also shown previously for Cu electrodes prepared by oxygen plasma.<sup>[73]</sup> The origin of the two black regions is discussed below.

Figure 9 shows SEM images taken on regions of the Cu wires removed directly after the electrolysis (left column) and kept in the solution for additional 60 s (center column). Figure S7 shows additional SEM images depicting a larger surface area. An SEM image of an as-prepared Cu electrode is provided in Figure S4b. The SEM images do not suggest distinct structural differences between both experimental approaches, even though both regions show slightly different colors in the optical microscope (Figure 8). Hence, the following description applies to both regions 1 and 3 depicted in Figure 8. In contrast to Pt and Au, the SEM images of Cu (Figure 9) demonstrate macroscopic surface structural changes as a function of the applied voltages. After electrolysis at low voltages (up to 100 V),

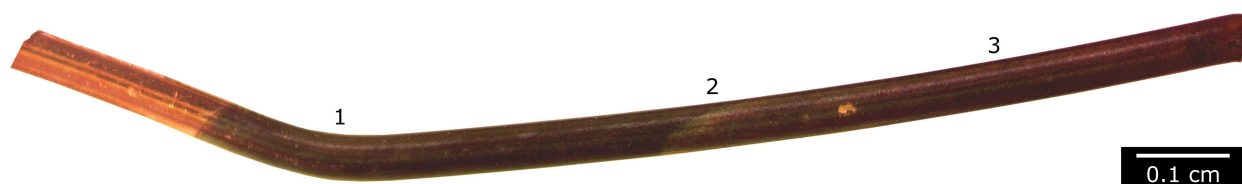


**Figure 8.** Microscope image of a Cu wire after electrolysis at 300 V for 30 s in 0.01 M KOH. The left part of the microscope image shows the as-prepared Cu wire. Region 1 shows the part of the wire which was immediately removed from the electrolyte after the electrolysis, where region 3 was obtained from keeping the electrode in the electrolyte for 60 s. Region 2 is the transition between region 1 and 3. The contrast and brightness of the image was visually improved for better visibility of the two regions.

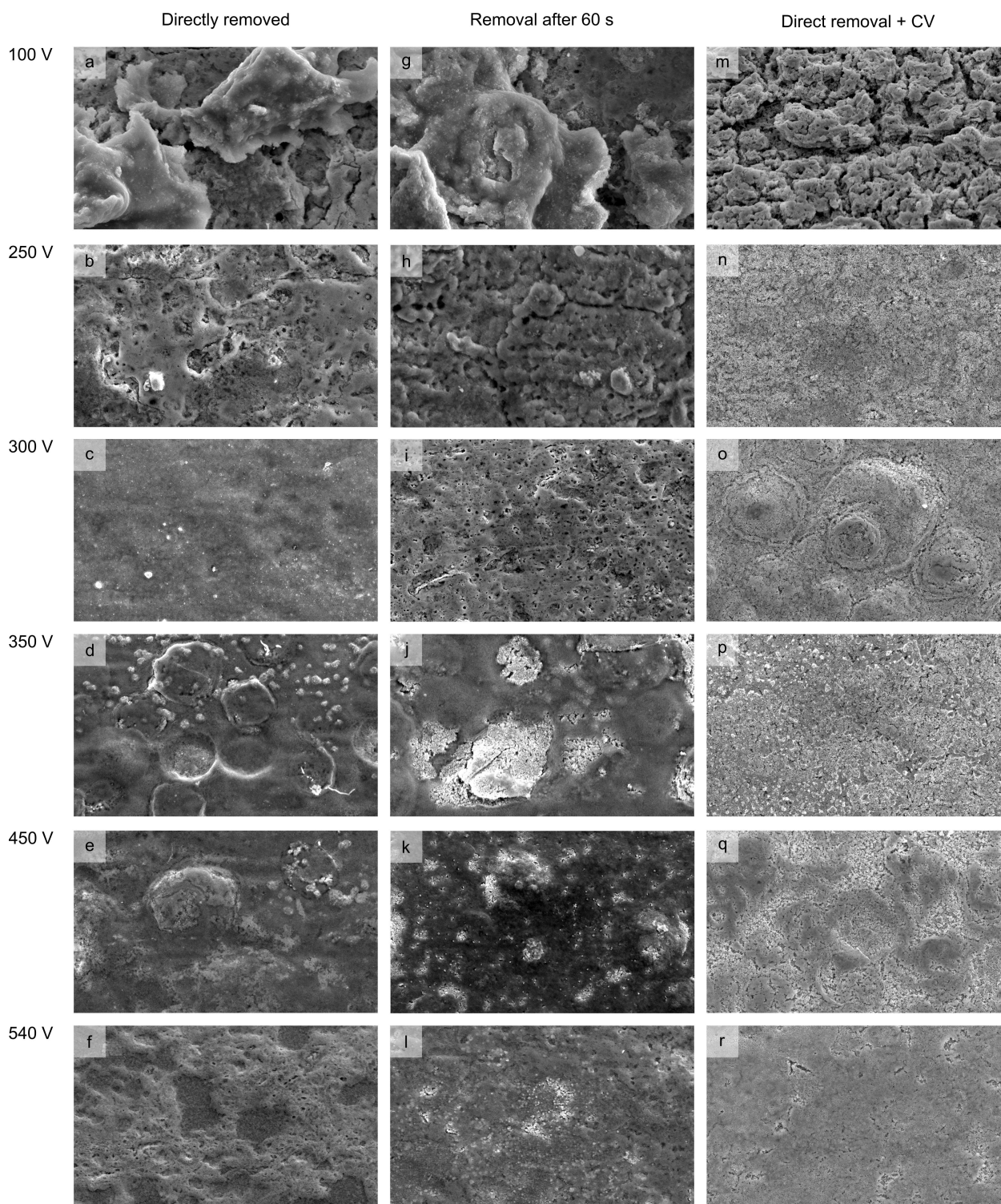


**Figure 9.** SEM images (50 μm × 30 μm) of Cu wire electrodes (length: 10 mm, diameter: 0.5 mm) after electrolysis at the given voltages for 30 s in 0.01 M KOH. The first column (a–f) shows micrographs of the surface structures of the wires that were directly removed after the electrolysis, the second column (g–l) after keeping them in the electrolysis solution for 60 s, and the third column (m–r) after direct removal of the wires and subsequent electrochemical characterization.

3D flake-like structures are formed. Three-dimensional macroscopic structure formation for Cu electrodes in alkaline media is not uncommon.<sup>[74–76]</sup> Performing electrolysis at intermediate

voltages (250 V) results in pitting of the surface. Performing electrolysis at high voltages, including the region for CGDE, the surface becomes more smooth.



As indicated above, the color change of the electrode during the electrolysis to black strongly implies that a CuO is formed. To quantify the amount of oxide, the electrodes were electrochemically reduced in 0.1 M KOH by sweeping the potential at  $50 \text{ mVs}^{-1}$  from 0.31 V to a potential beyond  $-0.2 \text{ V}$  and kept at a potential lower than  $-0.2 \text{ V}$  until the reduction current becomes insignificant (up to 40 s), as shown in Figure 10. After this procedure, the electrodes were completely reduced as confirmed by EDS measurements.<sup>[77]</sup> In principle, it is possible to determine the type of Cu oxide or hydroxide from the peak position in the negative-going scan direction of the CV.<sup>[76]</sup> However, in this case (see Figure 10) the amount of oxide is rather high such that distinct well-separated reduction peaks could not be resolved and the contribution from the reduction of different Cu oxides/hydroxides overlap. Nevertheless, based on the work by Deng and coworkers, who studied the OER in alkaline electrolyte, CuO was identified along with  $\text{Cu}^{\text{II}}\text{O}_2$  compounds by XANES and *in situ* Raman spectroscopy.<sup>[76]</sup> In combination with  $\text{K}^+$  or  $\text{Na}^+$ , such cuprates have a bluish-black color. From visual inspection, these compounds cannot be discerned. Electrochemically, it was suggested that the Cu(III) compounds could be reduced at potentials below 1.6 V and can be identified by a peak at potentials slightly below 1.6 V.<sup>[76]</sup> With our experimental approach, it is, however, not possible to identify the Cu(III) compounds since our starting potential (0.31 V) in the chronoamperometry measurements in Figure 10 is already below 1.6 V. Nevertheless, it is very likely that both Cu(II) and Cu(III) compounds form during the electrolysis at high voltages. Additional experiments are, however, required to confirm this assumption and elucidate the nature of the surface oxides formed.

In contrast to Au, independent of the pre-treatment, *i.e.*, direct removal of the electrodes after the electrolysis (Cu fast) or keeping the electrode in the electrolysis solution (Cu slow), a reduction current is measured on all Cu electrodes. The corresponding charge density passed during the electrochemical reduction of the electrodes (Figure 6) is depicted in Figure 1b for all investigated electrodes, along with the results obtained for Pt and Au. Overall, the charge density decreases

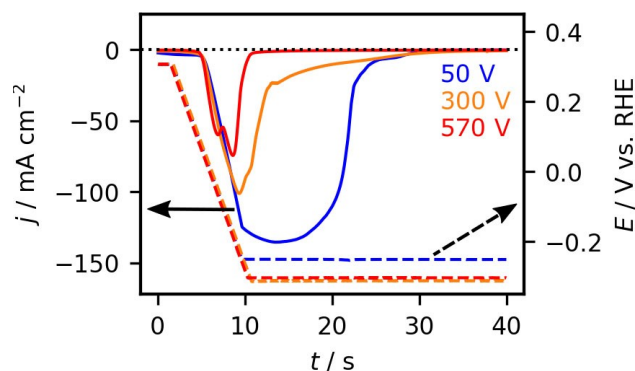


**Figure 10.** Characterization of the amount of oxide formed on Cu electrodes after the electrolysis at the given voltages, by sweeping the potential from 0.31 V to a potential beyond  $-0.2 \text{ V}$  until the cathodic current almost vanished.

almost exponentially with increasing applied voltage. In comparison to Au, the oxide formation is also still significant during CGDE.

For almost all electrolysis voltages in Figure 1c, it is apparent that the charge densities passed for the electrodes removed immediately after the electrolysis (Cu fast – red) are larger than those kept in the electrolysis solution (Cu slow – orange). Hence the electrodes are partially reduced when they are kept in the solution after electrolysis. Similar to the case of Au discussed above, we suggest that species in the electrolysis solution formed during the electrolysis, *i.e.*,  $\text{H}_2\text{O}_2$ , cause the reduction. Considering that Cu(III) compounds are formed during electrolysis (see above) and that these compounds are reduced at more positive potentials than the oxides that are reduced in the potential window of our electrochemical reduction experiment in Figure 10, we suggest that Cu(III) compounds are reduced to Cu(II) compounds under these conditions. Since the difference in charge density is small for both experimental procedures, it further implies that the amount of Cu(III) compounds formed during electrolysis is comparatively low.

The structural changes induced by the electrolysis and subsequent electrochemical reduction of the electrodes were investigated by cyclic voltammetry. The CV of an as-prepared electrode is shown in Figure 11a and b (black), and these

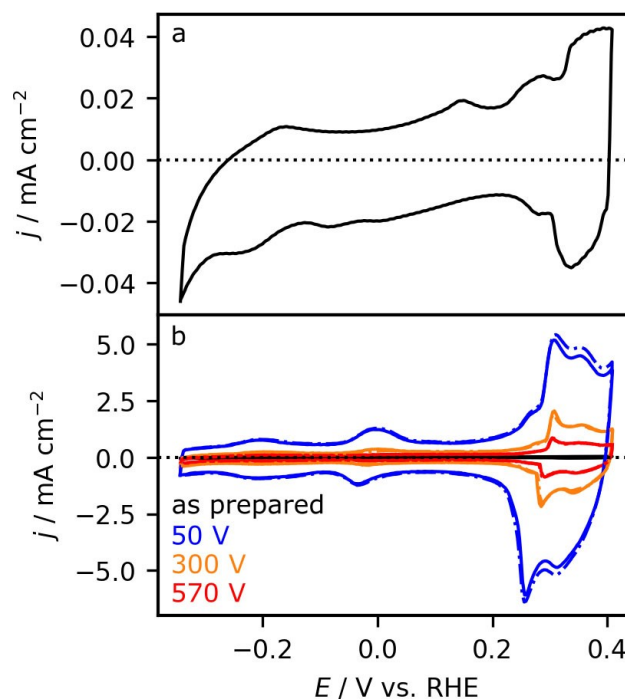


**Figure 11.** CVs of a) an as-prepared Cu wire in 0.1 M KOH (black) and b) the same electrode in comparison to the electrochemically reduced electrodes in Figure 10 (previously treated by electrolysis at the given voltages). The CVs were recorded at  $50 \text{ mVs}^{-1}$ . The CVs presented in b) with solid lines were measured after direct removal of the electrodes from the electrolysis solution and subsequent electrochemical reduction in Figure 10. In contrast, the CVs in dashed-dotted lines were recorded after keeping the electrodes in the electrolysis solution for 60 s and subsequent complete electrochemical reduction (reduction data not shown).

recorded after the electrolysis at 50, 300, and 570 V are shown in Figure 11b. In the latter, we also differentiate between electrodes, which were removed immediately from the electrolysis solution (solid lines), and those which were kept for additional 60 s in the electrolyte (dash-dotted lines). In general, for Cu electrodes the peaks at potentials larger than 0.2 V can be attributed to the formation and reduction of  $\text{Cu}_2\text{O}$ . The peaks at potentials smaller than 0.2 V can be attributed to surface OH adsorption and desorption on different low index surfaces.<sup>[78–81]</sup> From the comparison of the CVs of the as-prepared electrode with those recorded after electrolysis and subsequent reduction, it is apparent that the voltammetric features in the CV change, indicating that the crystallographic orientation of the electrode surface changed.<sup>[78]</sup> Interestingly, the characteristic features of the voltammograms recorded after electrolysis at different voltages are very similar for all electrodes, indicating that all electrodes have a similar surface crystallographic orientation. In addition, the RF of Cu increased in comparison to the as-prepared Cu electrodes shown in Figure 1c and is independent from the experimental procedure (immediate removal of the electrode after electrolysis or keeping the electrode in the electrolysis solution).

In turn, the RF decreases exponentially from 50 to 570 V, following the voltage-dependent evolution of the charge density. Note that for electrolysis in the CGDE region, the electrodes still have a six times larger surface area than the as-prepared Cu wire. The change in surface area is, to some extent, also apparent in the SEM images in Figure 9m–r (right column), where the surfaces became smoother with increasing voltage. Comparing the SEM images taken directly after the electrolysis (Figure 9g–l – middle column) with those taken after the electrochemical reduction (Figure 9m–r – right column) shows that the more rough surfaces obtained after electrolysis at low voltages stay rough after the electrochemical reduction (compare images in Figures 9a, g and m – first row). In a similar way the more flat surfaces obtained at high voltages also remain mostly flat after the electrochemical reduction (compare images in Figures 9f, l, and r – last row). Furthermore, SEM images taken at lower magnification in Figure S7 show, the formation of a porous structure after the electrochemical reduction. Overall, the structure formation of Cu is very similar to that observed for Au above, except that the oxide layer thickness and the porosity of the film shows a different voltage dependence.

### 3. Conclusions

In this work, we investigated the impact of electrolysis on the structural properties of Pt, Au, and Cu electrodes in a 0.01 M KOH solution in a voltage range from 50 to 580 V. We show that the  $I-U$  characteristics are mainly determined by the conductivity of the electrolyte or the gas film around the electrode at high voltages and that they are rather independent of the metal employed as well as the changes induced on the structural properties by the electrolysis. The difference in the structural properties has been explored by additional optical

microscope, SEM, and electrochemical measurements. The following key observations were made, and questions remain:

1. Pt seems to be stable during electrolysis in agreement with previous studies in different electrolytes. Whether or not the electrodes are restructured at an atomic level or dissolve partially during electrolysis, cannot be deduced from our measurements and is the subject of further investigations.
2. During electrolysis, an oxide film is formed on the Au and Cu electrodes, where the rate of formation depends on the metal and the applied voltage. The red color of the Au wire suggests that  $\text{Au}_2\text{O}_3$  is formed. In SEM images, the film appears rather flat and based on the charge density passed during the electrochemical reduction of the electrodes the oxide is thickest after electrolysis at the breakdown voltage of normal electrolysis (300 V). The black color of the Cu wire suggests that CuO is formed, which is rather textured (rough) and thickest for low voltages (50 V) and more flat and thinner in the CGDE region (540 V). Possible Cu(III) oxide formation, which was suggested to occur in the OER region under alkaline conditions, is very likely.<sup>[76]</sup> Further XPS measurements would be required to elucidate the oxidation state of the respective metals.
3. When the Au and Cu electrodes are kept for 60 s after the electrolysis in the electrolysis solution, their color changed from red to black for Au and from black to light black for Cu. Further electrochemical reduction measurements revealed that the Au oxide was completely and Cu oxide only partly reduced in the electrolysis solution. In the case of Cu, we suggest that the partial reduction is attributed to the reduction of Cu(III) compounds. The content of which is low and less stable than CuO or  $\text{Cu}_2\text{O}$ .<sup>[76]</sup> Our preliminary results to explain the reduction process on  $\text{Au}_2\text{O}_3$  suggest that  $\text{H}_2\text{O}_2$ , present in the electrolysis solution after the electrolysis, is at the origin of the oxide reduction. While it is known that  $\text{H}_2\text{O}_2$  is formed during CGDE,<sup>[11,17]</sup> the formation at lower voltages has so far not been considered.
4. Reducing the oxides formed during electrolysis, either by keeping the electrodes in the electrolysis solution (for Au) or reducing the oxide electrochemically (for Au and Cu), leads to the formation of a high surface area nanoporous film. The change in electrochemical surface area to the as-prepared electrodes follows the same trend as the charge density determined from the reduction experiments. In the case of Au, the final porous structure is also independent of the reduction procedure.

Overall, performing electrolysis at high voltages on Au and Cu can be used to form thick oxide layers on the electrodes. Based on our findings, the oxide structure and film thickness differ significantly for the different metals, and the oxide structure also depends on the applied voltage. Similarly, the surface area of the porous films depends on the applied voltage during electrolysis. Hence, if this approach was used to prepare oxide or porous films with specific film thickness on other metals, a systematic study of the whole voltage range is inevitable. Reasons for the voltage-dependent oxide growth rates still have to be elucidated. Note that it is also mandatory to remove the electrodes swiftly from the electrolysis solution

to assess properly the surface structures formed during electrolysis. Finally, such oxide-covered or highly-restructured materials with high surface area obtained from an initial electrolysis treatment could provide a new class of materials for possible applications as model electrodes in electrocatalysis, battery- and other energy-related research fields.

## Experimental Section

**Materials:** All aqueous solutions were prepared by mixing Milli-Q water (18.2 M $\Omega$  cm, TOC  $\leq$  3 ppb) with KOH pellets (99.99%, Sigma-Aldrich), 30% HCl (Merck, Suprapur) or 85% phosphoric acid (Merck, Suprapur).

Wires of Pt, Au, and Cu with a diameter of 0.5 mm were purchased from MaTeck (purity at least 99.99%).

**Sample preparation:** In the case of Pt and Au, the same electrodes were used for all experiments, which were freshly prepared for each measurement. Both electrodes were flame annealed for three minutes in a propane flame (MTI). In some cases, when the Au wire was strongly restructured during the electrolysis experiment, it was electropolished in 1 M HCl solution (10 V vs. a graphite counter electrode) and subsequently annealed for further three minutes in the propane flame.

In the case of Cu, a new wire was freshly prepared for each measurement. The Cu wires were sonicated in 85% phosphoric acid for one minute at room temperature to remove the native surface oxide layer. Subsequently, the Cu wires were thoroughly rinsed with Milli-Q water and dried in air.

**Electrolysis and electrochemical characterization:** The electrolysis experiments (NE and CGDE) and the electrochemical characterization were performed with separate cells. This was necessary since usually during the electrolysis, the electrolyte properties change, e.g., temperature and dissolved products such as H<sub>2</sub>, O<sub>2</sub>, and H<sub>2</sub>O<sub>2</sub>, which can affect the electrochemical characterization. All experiments were performed without stirring the electrolyte.

The electrolysis was performed in a glass cell containing 60 mL of 0.01 M KOH. A stainless steel plate of 15 mm  $\times$  20 mm  $\times$  3.5 mm was used as a counter electrode. The Pt and Au working electrode wires were immersed 10 mm into the electrolyte solution (4.5 or 10 mm for Cu) and were placed 2.5 cm apart from the counter electrode. The voltage for the electrolysis was applied for all electrodes for 30 s with a TDK-Lambda Power Supply (630 V/1.365 A) controlled via a LabVIEW software. Each electrolysis experiment was performed in a fresh electrolyte. The anode wire was either prepared again (Pt and Au), or a new electrode was used (Cu) to guarantee identical conditions for each experiment. For the presentation of the *I*-*U* plot in Figure 1, the data points were averaged for the 30 s electrolysis. The current density was determined from the geometric area of the wire electrode. During the 30 s electrolysis, the electrolyte temperature increases, leading to changes in the current density. Corresponding chronoamperometric curves are given in Figure S1 along with a more detailed description of the temperature effects. The measurements were repeated several times, and the values were averaged afterward. The error bars are derived from several experiments performed under similar conditions.

The electrochemical characterization of Pt and Au was performed in a glass beaker cell containing 150 mL of 0.01 M KOH. A homemade reversible hydrogen electrode (RHE) was used as a reference electrode and a Pt-sheet (10  $\times$  7.5 mm) as a counter electrode. All potentials are given on the RHE scale unless otherwise mentioned. The potential was controlled with a FHI ELAB potentiostat. The

electrochemical properties for Pt and Au electrodes were investigated before and after the electrolysis.

The initial scan direction in the CV was negative for Pt, starting from 0.95 V (close to the open circuit potential). Before the electrolysis, the potential window of the CV was fixed between 0.05 and 1.45 V. After electrolysis, first several cycles were recorded between 0.05 and 1.0 V to avoid significant surface restructuring. Subsequently, additional cycles with an upper potential limit of 1.45 V were recorded for comparison with the last CV recorded before the electrolysis.

The initial scan direction was negative for Au, starting from 1.1 V. The CVs were recorded in a potential window of 0.20 to 1.69 V. After the electrolysis, the surface was reduced electrochemically by holding the potential at 0.25 V in the first negative scan until the reduction currents became insignificant. The resulting charge densities are discussed in the manuscript.

For Cu, the electrochemical characterization was performed in a conventional three-electrode glass cell in 0.1 M KOH with a Hg/HgO reference electrode (RE-61AP, ALS) and a graphite rod as a counter electrode. The potential was controlled with a HEKA PG510 potentiostat. The starting potential to record the Cu CVs was 0.31 V, and the potential window was  $-0.34$  V to 0.41 V. The characterization by cyclic voltammetry before the electrolysis was only performed on a few samples to ensure that the preparation procedure yielded reproducible CVs and hence similar surface structures. After the electrolysis, the surface oxide was reduced by holding the electrode at potentials lower than  $-0.2$  V until the current densities related to oxide reduction became insignificant.

**Surface area:** All current densities are related to the original geometric surface area (Pt, Au: 0.16 cm<sup>2</sup>, Cu: 0.07 or 0.16 cm<sup>2</sup>) of the electrodes, determined from the length and diameter of the wires.

**Charge density:** The oxide formed on Au and Cu during electrolysis was reduced by scanning at 50 mVs<sup>-1</sup> from the starting potential of the CV (see above) to the lower potential limit and keeping the electrode at that potential until the cathodic currents disappeared. The charge density is obtained from integrating the current density, which in turn corresponds to the amount of oxide formed on the electrode. Note that a small fraction of the charge density might also be related to the reduction of residual molecular oxygen dissolved in the electrolyte. These currents are, however, small compared to the oxide reduction currents. The charge density is related to the geometric surface area deduced from the as-prepared electrodes, and it is a measure of the oxide thickness, which will be discussed in more detail elsewhere.

**Roughness factor – RF:** For all materials, we determined the increase in surface area from the current in the double-layer region of the CVs recorded at a scan rate of 50 mVs<sup>-1</sup> before and after electrolysis. This ratio is denoted as roughness factor (RF). The evaluation was performed on CVs where neither Faraday reactions nor adsorption processes occur before and after the electrolysis (or electrochemical reduction).<sup>[55]</sup> The respective potentials from which the RF was determined are 0.87 V for Au, 0.50 V for Pt, and  $-0.24$  V for Cu. The last recorded CV before the electrolysis contained the information on the RF before the electrolysis. Direct information on the RF of Au and Cu after the electrolysis is not accessible since the oxide reduction currents strongly overlap with the double layer region in the CV. Therefore, we determined the RF after the electrolysis from the last CV recorded after the complete reduction of the surface. Note that strictly speaking, this approach reveals the increase in electrochemical active surface area. Also, since the RF describes a ratio between the initial and final roughness, information on the absolute surface roughness cannot be determined with this approach.

**Structural characterization:** The morphology and microscopic structural properties of the wires were investigated using a Quattro S scanning electron microscope (SEM) from Thermo Scientific operating at an acceleration voltage of 10 or 20 kV. The optical microscope images were taken with the Leica S9i.

## Author Contributions

E. Artmann: Conceptualization, Formal Analysis, Funding Acquisition, Investigation, Validation, Visualization, Writing – Original Draft Preparation; P. V. Menezes: Investigation, Writing – Review & Editing; L. Forschner: Investigation, Writing – Review & Editing; M. M. Elnagar: Investigation, Writing – Review & Editing; L. A. Kibler: Writing – Review & Editing; T. Jacob: Funding Acquisition, Resources, Supervision, Writing – Review & Editing; A. K. Engstfeld: Conceptualization, Supervision, Writing – Review & Editing.

## Acknowledgements

This work was supported by the Deutsche Forschungsgemeinschaft (DFG) through Grant No. SFB-CRC1316 (collaborative research center). EA would like to thank the “Stiftung Stipendien-Fonds des Verbandes der Chemischen Industrie (VCI)” for the financial support provided by a Kekulé scholarship. Open Access funding enabled and organized by Projekt DEAL.

## Conflict of Interest

The authors declare no conflict of interest.

**Keywords:** alkaline electrolyte · contact glow discharge electrolysis · electrode stability · electrolysis · plasma chemistry

- [1] A. Yerokhin, V. R. Mukaeva, E. V. Parfenov, N. Laugel, A. Matthews, *Electrochim. Acta* **2019**, *312*, 441–456.
- [2] K. Uosaki, *Electrochemical Science for a Sustainable Society: A Tribute to John O'M Bockris*, Springer, **2017**.
- [3] W. Schmickler, E. Santos, *Interfacial electrochemistry*, Springer Science & Business Media, **2010**.
- [4] G. Yang, B. Wang, K. Tawfiq, H. Wei, S. Zhou, G. Chen, *Surf. Eng.* **2017**, *33*, 149–166.
- [5] P. J. Bruggeman et al., *Plasma Sources Sci. Technol.* **2016**, *25*, 053002.
- [6] P. N. Belkin, S. A. Kusmanov, E. V. Parfenov, *Appl. Surf. Sci.* **2020**, *1*, 100016.
- [7] S. Horikoshi, N. Serpone, *RSC Adv.* **2017**, *7*, 47196–47218.
- [8] A. I. Yanson, P. Rodriguez, N. Garcia-Araez, R. V. Mom, F. D. Tichelaar, M. T. M. Koper, *Angew. Chem. Int. Ed.* **2011**, *50*, 6346–6350; *Angew. Chem.* **2011**, *123*, 6470–6474.
- [9] G. Saito, T. Akiyama, *J. Nanomater.* **2015**, *2015*, 1–21.
- [10] H. H. Kellogg, *J. Electrochem. Soc.* **1950**, *97*, 133.
- [11] A. Hickling, M. D. Ingram, *Trans. Faraday Soc.* **1964**, 783–793.
- [12] S. K. Sen Gupta, R. Singh, *Plasma Sources Sci. Technol.* **2017**, *26*, 015005.
- [13] X. Jin, X. Wang, J. Yue, Y. Cai, H. Zhang, *Electrochim. Acta* **2010**, *56*, 925–928.
- [14] K. Azumi, T. Mizuno, T. Akimoto, T. Ohmori, *J. Electrochem. Soc.* **1999**, *146*, 3374–3377.
- [15] A. L. Yerokhin, X. Nie, A. Leyland, A. Matthews, S. J. Doney, *Surf. Coat. Technol.* **1999**, *122*, 73–93.
- [16] S. K. Sengupta, O. P. Singh, *J. Electroanal. Chem. Interfacial Electrochem.* **1991**, *301*, 189–197.
- [17] S. K. Sengupta, O. P. Singh, *J. Electroanal. Chem.* **1994**, *369*, 113–120.
- [18] B. Zheng, K. Wang, M. Shrestha, T. Schuelke, Q. H. Fan, *Plasma Sources Sci. Technol.* **2019**, *28*, 085016.
- [19] D. Landolt, *Electrochim. Acta* **1987**, *32*, 1–11.
- [20] N. Arulmozhi, T. J. P. Hersbach, M. T. M. Koper, *Proc. Natl. Acad. Sci. USA* **2020**, *117*, 32267–32277.
- [21] M. M. Elnagar, J. M. Hermann, T. Jacob, L. A. Kibler, *Electrochim. Acta* **2021**, *372*, 137867.
- [22] M. M. Elnagar, J. M. Hermann, T. Jacob, L. A. Kibler, *Curr. Opin. Electrochem.* **2021**, *27*, 100696.
- [23] S. K. Sen Gupta, *Plasma Chem. Plasma Process.* **2017**, *37*, 897–945.
- [24] T. W. Clyne, S. C. Troughton, *Int. Mater. Rev.* **2019**, *64*, 127–162.
- [25] X. Lu, M. Mohedano, C. Blawert, E. Matykina, R. Arrabal, K. U. Kainer, M. L. Zheludkevich, *Surf. Coat. Technol.* **2016**, *307*, 1165–1182.
- [26] G. Barati Darband, M. Aliofkhaezaei, P. Hamghalam, N. Valizade, *J. Magnes. Alloys* **2017**, *5*, 74–132.
- [27] K. Nestler, F. Böttger-Hiller, W. Adamitzki, G. Glowa, H. Zeidler, A. Schubert, *Procedia Chem.* **2016**, *42*, 503–507.
- [28] T. A. Kareem, A. A. Kalliani, *Ionics* **2012**, *18*, 315–327.
- [29] A. Allagui, Z. Said, M. A. Abdelkareem, A. S. Elwakil, M. Yang, H. D. C. Alawadhi, *J. Electrochem. Soc.* **2017**, *164*, A2539–A2546.
- [30] A. Allagui, E. A. Baranova, R. Wüthrich, *Electrochim. Acta* **2013**, *93*, 137–142.
- [31] Y. Toriyabe, S. Watanabe, S. Yatsu, T. Shibayama, T. Mizuno, *Appl. Phys. Lett.* **2007**, *91*, 041501.
- [32] G. Saito, Y. Nakasugi, T. Yamashita, T. Akiyama, *Nanotechnology* **2014**, *25*, 135603.
- [33] F. Kurniawan, R. Rahmi, *Bull. Chem. React. Eng. Catal.* **2017**, *12*, 281.
- [34] Q. Chen, J. Li, Y. Li, *J. Phys. D* **2015**, *48*, 424005.
- [35] M. A. Malik, A. Ghaffar, S. A. Malik, *Plasma Sources Sci. Technol.* **2001**, *10*, 82–91.
- [36] X. Wang, M. Zhou, X. Jin, *Electrochim. Acta* **2012**, *83*, 501–512.
- [37] J. Gao, X. Wang, Z. Hu, H. Deng, J. Hou, X. Lu, J. Kang, *Water Res.* **2003**, *37*, 267–272.
- [38] J. Pettersson, B. Ramsey, D. Harrison, *J. Power Sources* **2006**, *157*, 28–34.
- [39] E. Antolini, *J. Appl. Electrochem.* **2004**, *34*, 563–576.
- [40] J. K. Nørskov, T. Bligaard, A. Logadottir, J. R. Kitchin, J. G. Chen, S. Pandalov, U. Stimming, *J. Electrochem. Soc.* **2005**, *152*, J23–J26.
- [41] V. Climent, J. M. Feliu, *J. Solid State Electrochem.* **2011**, *15*, 1297–1315.
- [42] S. Trasatti, *J. Electroanal. Chem. Interfacial Electrochem.* **1972**, *39*, 163–184.
- [43] B. Hammer, J. K. Nørskov, *Nature* **1995**, *376*, 238–240.
- [44] L. D. Burke, *Gold Bull.* **2004**, *37*, 125–135.
- [45] G. Tremiliosi-Filho, L. H. Dall'Antonia, G. Jerkiewicz, *J. Electroanal. Chem.* **1997**, *422*, 149–159.
- [46] Y. Hori, in *Modern Aspects of Electrochemistry*, Eds. C. G. Vayenas, R. E. White, M. E. Gamboa-Aldeco, Springer, New York, **2008**, vol. 42, pp. 89–189.
- [47] D. Gao, I. Zegkinoglou, N. J. Divins, F. Scholten, I. Sinev, P. Grosse, B. Roldan Cuenya, *ACS Nano* **2017**, *11*, 4825–4831.
- [48] S. Nitopi, E. Bertheussen, S. B. Scott, X. Liu, A. K. Engstfeld, S. Horch, B. Seger, I. E. L. Stephens, K. Chan, C. Hahn, J. K. Nørskov, T. F. Jaramillo, I. Chorkendorff, *Chem. Rev.* **2019**, *119*, 7610–7672.
- [49] S. Yatsu, H. Takahashi, H. Sasaki, N. Sakaguchi, K. Ohkubo, T. Muramoto, S. Watanabe, *Arch. Metall. Mater.* **2013**.
- [50] H. Tsai, E. Hu, K. Perng, M. Chen, J.-C. Wu, Y.-S. Chang, *Surf. Sci.* **2003**, *537*, L447–L450.
- [51] S. Popović, M. Smiljanić, P. Jovanović, J. Vavra, R. Buonsanti, N. Hodnik, *Angew. Chem. Int. Ed.* **2020**, *59*, 14736–14746; *Angew. Chem.* **2020**, *132*, 14844–14854.
- [52] R. Akolkar, R. M. Sankaran, *J. Vac. Sci. Technol. A* **2013**, *31*, 050811.
- [53] P. Mandin, R. Wüthrich, H. Roustan, *AIChE J.* **2010**, *33*, 2446–2454.
- [54] L. A. Kibler, *Int. Soc. Electrochem.* **2003**, 1–55.
- [55] M. Lukaszewski, *Int. J. Electrochem. Sci.* **2016**, 4442–4469.
- [56] P. Daubinger, J. Kieninger, T. Unmüssig, G. A. Urban, *Phys. Chem. Chem. Phys.* **2014**, *16*, 8392–8399.
- [57] K. Itaya, S. Sugawara, K. Sashikata, N. Furuya, *J. Vac. Sci. Technol. A* **1990**, *8*, 515–519.
- [58] N. Arulmozhi, D. Esau, R. P. Lamsal, D. Beauchemin, G. Jerkiewicz, *ACS Catal.* **2018**, *8*, 6426–6439.

- [59] L. Jacobse, Y.-F. Huang, M. T. M. Koper, M. J. Rost, *Nat. Mater.* **2018**, *17*, 277–282.
- [60] T. Fuchs, J. Drnec, F. Calle-Vallejo, N. Stubb, D. J. S. Sandbeck, M. Ruge, S. Cherevko, D. A. Harrington, O. M. Magnussen, *Nat. Catal.* **2020**, *3*, 754–761.
- [61] S. K. Sengupta, *J. Electrochem. Soc.* **1998**, *145*, 2209.
- [62] X.-L. Jin, X.-Y. Wang, H.-M. Zhang, Q. Xia, D.-B. Wei, J.-J. Yue, *Plasma Chem. Plasma Process.* **2010**, *30*, 429–436.
- [63] U. Gangal, M. Srivastava, S. K. Sen Gupta, *J. Electrochem. Soc.* **2009**, *156*, F131.
- [64] Z. Li, P. Beck, D. A. Ohlberg, D. R. Stewart, R. S. Williams, *Surf. Sci.* **2003**, *529*, 410–418.
- [65] M. Favaro, C. Valero-Vidal, J. Eichhorn, F. M. Toma, P. N. Ross, J. Yano, Z. Liu, E. J. Crumlin, *J. Mater. Chem. A* **2017**, *5*, 11634–11643.
- [66] B. Kirchhoff, L. Braunwarth, C. Jung, H. Jónsson, D. Fantauzzi, T. Jacob, *Small* **2020**, *16*, e1905159.
- [67] G. Jerkiewicz, G. Tremiliosi-Filho, B. E. Conway, *J. Electroanal. Chem.* **1992**, *334*, 359–370.
- [68] F. Widdascheck, M. Kothe, A. A. Hauke, G. Witte, *Appl. Surf. Sci.* **2020**, *509*, 145039.
- [69] A. Stadnichenko, S. Koshcheev, A. Boronin, *Moscow Univ. Chem. Bull.* **2007**, *62*, 343–349.
- [70] A. Sukeri, M. Bertotti, *J. Braz. Chem. Soc.* **2018**, *29*, 226–231.
- [71] A. Vitrey, R. Alvarez, A. Palmero, M. U. González, J. M. García-Martín, *Beilstein J. Nanotechnol.* **2017**, *8*, 434–439.
- [72] H. Zheng, C. Picard, S. Ravaine, *Front. Chem. Sci. Eng.* **2018**, *12*, 247–251.
- [73] H. Mistry, A. S. Varela, C. S. Bonifacio, I. Zegkinoglou, I. Sinev, Y.-W. Choi, K. Kisslinger, E. A. Stach, J. C. Yang, P. Strasser, B. Roldan Cuenya, *Nat. Commun.* **2016**, *7*, 1–9.
- [74] A. Vvedenskii, S. Grushevskaya, S. Ganzha, D. Eliseev, *J. Solid State Electrochem.* **2014**, *18*, 2755–2770.
- [75] A. Vvedenskii, S. Grushevskaya, S. Ganzha, D. Eliseev, L. I. Abakumova, *J. Solid State Electrochem.* **2014**, *18*, 3437–3451.
- [76] Y. Deng, A. D. Handoko, Y. Du, S. Xi, B. S. Yeo, *ACS Catal.* **2016**, *6*, 2473–2481.
- [77] P. V. Menezes, M. M. Elnagar, M. Al-Shakran, M. Eckl, P. W. Menezes, L. A. Kibler, T. Jacob, *Adv. Funct. Mater.* **2021**, accepted.
- [78] A. K. Engstfeld, T. Maagaard, S. Horch, I. Chorkendorff, I. E. L. Stephens, *Chem. Eur. J.* **2018**, *24*, 17743–17755.
- [79] K. J. P. Schouten, E. P. Gallent, M. T. M. Koper, *Journal of Electroanalytical Chemistry* **2013**, *699*, 6–9.
- [80] A. Bagger, R. M. Arán-Ais, J. Halldin Stenlid, E. Campos Dos Santos, L. Arnarson, K. Degn Jensen, M. Escudero-Escribano, B. Roldan Cuenya, J. Rossmeisl, *ChemPhysChem* **2019**, *20*, 3096–3105.
- [81] A. Tiwari, H. H. Heenen, A. S. Bjørnlund, T. Maagaard, E. Cho, I. Chorkendorff, H. H. Kristoffersen, K. Chan, S. Horch, *J. Phys. Chem. Lett.* **2020**, *11*, 1450–1455.

---

Manuscript received: June 6, 2021

Revised manuscript received: August 10, 2021

Accepted manuscript online: September 14, 2021

Version of record online: November 2, 2021